Reference: *Biol. Bull.* **187:** 156–163. (October, 1994)

Locomotion in Developing *Artemia* Larvae: Mechanical Analysis of Antennal Propulsors Based on Large-Scale Physical Models

TERRI A. WILLIAMS*

Department of Zoology NJ-15, University of Washington, Seattle, Washington 98195

Abstract. A physical model of the swimming appendage (second antenna) of a larval *Artemia* was oscillated and translated through a tank of glycerine to determine how such a shape may be used to generate thrust at the intermediate Reynolds numbers at which it operates. Force on the model was measured by strain gauges and used to calculate coefficients of drag at a series of speeds and frequencies that represented flow regimes of different larval stages. Measured coefficients of drag (C_d) over this Reynolds number range (~1–10) suggest that an expression for a cylinder perpendicular to flow at intermediate Reynolds number ($C_d = 1 + 10\ Re^{-2/3}$) best represents the changes in drag coefficients for this geometry.

Unsteady forces were found to be a negligible portion of the force on the model in spite of a high ratio of frequency of oscillation to forward translational velocity (*i.e.*, Strouhal number).

Comparison of the thrust generated by the model with its fan of setae rigidly fixed *versus* passively flexing suggests that passive extension of setae can be influenced by relative limb and body speed.

Introduction

Animals that swim span an enormous range of sizes. This range is so great that the hydrodynamics that governs propulsion of the very small, slow swimmers and the large, fast swimmers are quite different. Small swimmers contend only with the viscosity of the fluid around them: flows are reversible, and shape does not greatly affect the pattern of flow. By contrast, large, fast swimmers use the inertial properties of fluids for propulsion: bodies are streamlined to reduce pressure drag, and propulsion is often achieved by accelerations of the surrounding fluid.

We understand the principles that determine these extreme cases because theoretical fluid dynamics provides solutions to the Navier-Stokes equations for these extremes: at the low end, inertial effects of the fluid are neglected; at the high end, viscous effects are neglected. But many organisms exist between these two extremes, and the flows they experience are a result of both fluid viscosity and fluid inertia. Planktonic animals are a good example of a whole category of organisms that inhabit this fluid regime. They include not only adults but also the larval stages of many animals.

Larvae are particularly interesting because, unlike their adult counterparts, they undergo changes in size and shape. This means that early in its life cycle an animal can be moving in a fluid regime dominated by viscosity and then, as it grows and develops, can experience flows that result from an increase in the importance of inertial effects. The brine shrimp, *Artemia*, provides such an example. Larvae swim actively from hatching until maturity. They are about 0.5 mm long when they hatch and swim at an average speed of 2 mm/s using only one pair of limbs. These limbs, the antennae, dominate propulsion during the first half of larval life and are gradually succeeded by a series of limbs that develop sequentially on the trunk. During part of the larval development of *Artemia*, the antennae increase in length from 0.25 mm to 0.50 mm, and the frequency of limb beat drops from 9.5 Hz to 8.0 Hz. Reynolds numbers of the limb based on limb length range from 1 to 9, and Strouhal numbers based on average body velocity drop from 8 to 3 (Table I). The antennae are used in a paddling mode of propulsion throughout this period of growth and change of form.

Received 4 June 1993; accepted 19 July 1994.

* Present address: Department of Anatomy, University of Vienna, Währingerstrasse 13, A-1090 Wien, Austria.

Table 1

Parameters used to model limb beat in selected larval stages, and forces measured on model limb

Stage	Antennal length (mm)	Freq. (Hz)	Body speed (mm s^{-1})	Re	St	Re model	St model	σ from eqn. 5	σ from eqn. 6	Drag-based force (N)	Unsteady force (N)
A) nauplius	0.24	9.5	1.8	1	8	2	5	0.16	0.14	5.7×10^{-2}	4.5×10^{-4}
B) limb bud	0.30	9.0	3.0	3	6	3	6	0.10	0.09	1.2×10^{-1}	1.3×10^{-3}
C) 4 trunk limbs	0.40	8.3	8.4	7	3	5	3	0.09	0.10	3.9×10^{-1}	3.5×10^{-3}
D) 7 trunk limbs	0.50	8.0	8.0	9	3	6	4	0.14	0.10	4.3×10^{-1}	4.8×10^{-3}

How does the balance of forces that determine movement change as the animal grows? Neither viscosity nor inertia dominate in determining the movements of *Artemia* larvae and other small crustaceans. Because both these effects must be accounted for, the Navier-Stokes equations of motion cannot be simplified to provide an analytical solution for force production. Existing models and measures of propulsion in small crustaceans import equations from engineering based on flow past geometric shapes at intermediate Reynolds numbers (*e.g.*, Morris *et al.*, 1985). I test the applicability of such equations by actual force measurements on a large-scale physical model of a larval *Artemia* antenna.

Because larvae are too small (~1 mm) for direct force measurements, I built a physical model of the limb which could both translate and oscillate through a tank of glycerin. For a series of larval stages, I preserved relevant fluid parameters based on kinematics measured from high-speed cine-photography and the morphology of the limbs. By mimicking the change in hydrodynamic regime these limbs experience during the development of *Artemia*, I estimated forces for a variety of stages and inspected how the growth of inertial effects influences force generation through development. In addition to assessing the overall importance of inertial effects, I tested the importance of unsteady or accelerational fluid forces in these high-frequency oscillating propulsors of developing larvae. These results are used in a theoretical model of rowing propulsion that can be directly compared to kinematic sequences of *Artemia* larvae taken with high-speed cine-photography (Williams, 1994).

Materials and Methods

Fluid forces and dynamic modeling

The force due to drag on an object moving through fluid at a constant velocity can be written:

$$\text{force} = 1/2\rho S(U)^2 C_d \qquad (1)$$

where ρ is the density of the fluid, S is the area of the object, U is the velocity of the object, and C_d is the coefficient of drag (defined below). This general expression applies to both viscous and inertia-dominated flow conditions. However, drag is generated differently in the two situations, and this will be reflected by the expression that defines the coefficient of drag, C_d. To determine an expression for C_d in the hydrodynamic regimes that the larvae experience, I measure drag directly on a large-scale physical model (see below) and calculate a value for C_d based on the average of the values calculated throughout a single stroke cycle of this model.

This expression for drag describes the force generated in a steady or time-invariant flow but, when inertial effects are important, an additional force may arise. This is the unsteady or added mass force that depends on the reaction of fluids to acceleration.

I assess the relative role of the unsteady forces in two ways. First, I compare thrust produced by the model with thrust predicted on the basis of steady and unsteady forces. I calculate this unsteady force, G, using:

$$G = \text{acceleration reaction} = \alpha\rho(V)dU/dt \qquad (2)$$

where α is the added-mass coefficient, a shape-dependent factor that is close to 1.0 (Daniel, 1984), V is the volume of the object, and U is its speed. I then compare the relative magnitudes of the steady and unsteady forces in the total force produced to gauge, theoretically, the importance of unsteady forces.

Second, I compare thrust produced by the model with a theoretical thrust calculated only on the basis of the angular position of the model as if it were oscillating without translating. If there are no unsteady effects, these two measures of thrust should be in phase; *i.e.*, the forces generated by translation and those generated by oscillation should add in a linear fashion.

Scaling of the model

I used two indices to mimic the hydrodynamic regime of a beating *Artemia* limb, Reynolds and Strouhal numbers. Both are dimensionless numbers that encapsulate certain features of the fluid environment.

The Reynolds number (Re) is defined as

$$Re = \rho \ell U_a / \mu \quad (3)$$

where ρ = fluid density, ℓ = some characteristic linear dimension of the object, in this case the length of the limb, U_a = average speed, and μ = viscosity of the fluid. For objects of the same geometry, equality of Reynolds number implies equality of the pattern of flow and equality of drag coefficients. My physical model can preserve these two features of an *Artemia* antenna, assuming that it represents the important features of antennal geometry.

However, the limbs oscillate. The Strouhal number (= reduced frequency parameter) is another dimensionless index that characterizes the flow. Conservation of this parameter implies conservation of the relative importance of fluid acceleration to steady flows. Strouhal number (St) is defined as

$$St = \omega \ell / U_b \quad (4)$$

where ω is the angular frequency of the limb, ℓ is the length of the limb, and U_b is the average velocity of the body.

I chose speeds and frequencies to drive the large-scale physical model of *Artemia* antenna that would approximate the combination of Re and St of the beating antenna at four selected larval stages. These are based on high-speed cine-photography and therefore do not account for stage-specific variation in larvae (see companion paper for discussion; Williams, 1994).

Measurement of force coefficients

Simple translation of the physical model (see below) yielded only a very limited range of speeds for direct measurements of drag coefficients. To evaluate the drag coefficients over a broader, more biologically relevant range, I calculated an average drag coefficient for the different trial runs (in which the model both translated and oscillated, see *Fluid forces and dynamic modeling*, above). The higher velocities resulting from the combined speed of translation and speed of oscillation yielded a broader range of Reynolds numbers. I compare the coefficient of drag calculated this way to two, different expressions for the coefficient of drag (C_d) of a cylinder perpendicular to flow: either

$$C_d = 24/Re \quad (5)$$

which expresses the low Reynolds number linear dependence of force on speed (Batchelor, 1967), or

$$C_d = 1 + 10(Re^{-2/3}) \quad (6)$$

which allows for the growth of pressure drag at intermediate Reynolds number situations, $1 < Re < 1 \times 10^5$ (White, 1974).

I also evaluated which expression for C_d better predicts the actual thrust produced by the model by comparing thrust predicted on the basis of either expression with measured thrust. I used the expression for standard deviation (Sokal and Rohlf, 1981), σ, as a measure of fit between the measured and predicted curves:

$$\sigma = [1/n \; \Sigma \; (t_c - t_m)^2]^{1/2} \quad (7)$$

where n is the number of points, t_c is the calculated thrust, and t_m is the measured thrust. See Williams (1994) for the details of calculating thrust.

The physical model and driving apparatus

A physical model of a limb that could be propelled within a tank of glycerin mimicked certain features of the active *Artemia* antennae. For the geometry of the model limb (*i.e.*, limb shape and setal spacing), I used direct tracings from film sequences of free-swimming animals (Williams, 1994). The model was constructed with casting resin. Thin brass cylinders formed a fixed fan that flexibly attached to the distal edge of the model (Fig. 1). This allowed the fan to flex during the recovery stroke; a raised lip in the cast itself anchored the fan in an extended position during the power stroke. Alternatively, the fan could be anchored in place so that it remained extended in both power and recovery strokes. This allowed comparison between a symmetrical and a passively asymmetrical stroke.

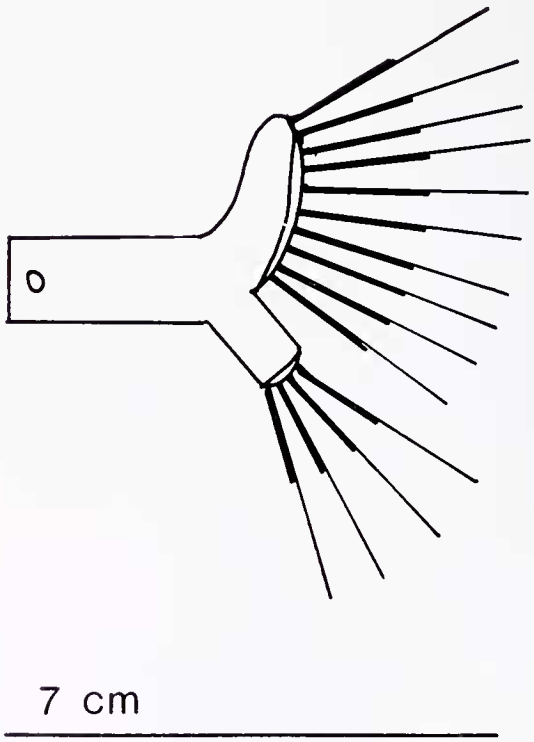

Figure 1. Cast resin model of *Artemia* larval antenna. Setal fan built of fine brass and tungsten wire.

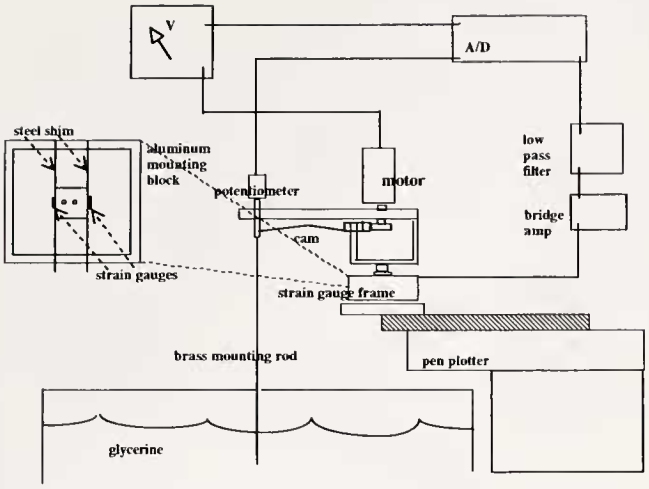

Figure 2. Apparatus used for measuring thrust of the model of *Artemia* larval antenna. The mounting carriage translates along an axis perpendicular to the plane of the page. The strain gauge frame is seen in planar view to the left of the diagram. (V = voltage; A/D = analog to digital.)

The model was attached to the end of a long, thin, brass rod that extended into a 50-gallon tank of glycerine (Fig. 2). The model rode in the middle of the tank approximately six model-lengths to the sides of the tank and seven to the bottom. The model limb could oscillate and translate independently at various speeds and frequencies. A modified pen plotter (Houston Instruments, Omnigraphic), controlled directly by a computer, translated the limb at speeds ranging from 1.2 cm s^{-1} to 6.0 cm s^{-1}. A rotating cam, driven by a small motor connected to the base of the brass rod, swung the limb in a 100° arc in an oscillating manner. A potentiometer documented the position of the model in the cycle. Frequencies ranged from 0.15 Hz to 0.55 Hz.

Two opposing 350-ohm semiconductor strain gauges (Entran), aligned perpendicular to the direction of thrust, measured displacement. I calibrated the force required to yield these displacements by hanging a series of small weights, 0.5–20 g, from the aluminum block between the two strain gauges (planar view of strain gauge frame: see Fig. 2, strain gauge frame). From this, I calculated a relationship between force and voltage. The response of the strain gauges was linear for the displacements I measured. The signal was amplified by a Gould bridge amplifier and filtered with a Krohn-Hite variable filter. Low-pass filtering with a 10-Hz cutoff removed the mechanical and other high-frequency noise caused by translating the model down the plotter. This cutoff introduced a slight phase shift (8°) in the signal at the high end of experimental frequencies. I corrected for the phase shift in computations of the phase between measured force and speed of the model.

The apparatus automatically repeated runs at each particular speed and frequency 100 times so that an average signal for thrust was obtained. In order to subtract drag of the brass rod from the experimental runs, I measured drag on the brass rod alone at the appropriate speeds.

Results

Average coefficients of drag calculated from thrust produced during trials in which the speed and frequency of the model is scaled to mimic four ontogenetic stages are plotted along with C_d predicted from equations 5 and 6 (Fig. 3). Average values for C_d follow almost exactly those predicted for a circular cylinder normal to flow at intermediate Reynolds numbers. In addition, values of the standard deviation, σ, between thrust produced by the model and thrust calculated on the basis of these two different expressions for C_d, confirm that, in three of four cases, the model generates thrust roughly as a cylinder at intermediate Reynolds numbers (Table I). The measured thrust per stroke of the model is compared in Figure 4 with thrust calculated on the basis of equation 6.

Two measures show the absence of unsteady forces on the model. First, in the calculation of thrust, the unsteady effects are two orders of magnitude lower than drag-based effects in all stages examined (Table I). Second, the time-course of thrust production can be predicted simply by the angular position of the model. Figure 5 compares thrust generated by the model with thrust calculated on the basis of angular position only. The difference between the measured thrust and such predicted thrust is simply due to the drag imposed by towing the model; there is no phase lag that would indicate unsteady effects. The difference is greater in the simulations of later stages where the towing speed is greater.

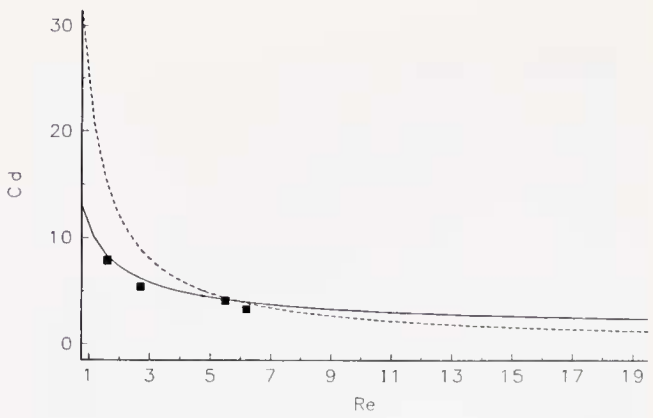

Figure 3. Relationship between drag coefficient (C_d) and Reynolds number (Re) for eqn. 5 (dotted line) and eqn. 6 (solid line). Filled squares represent the average C_d calculated from measured thrust of the model during different trials consisting of 100 runs each.

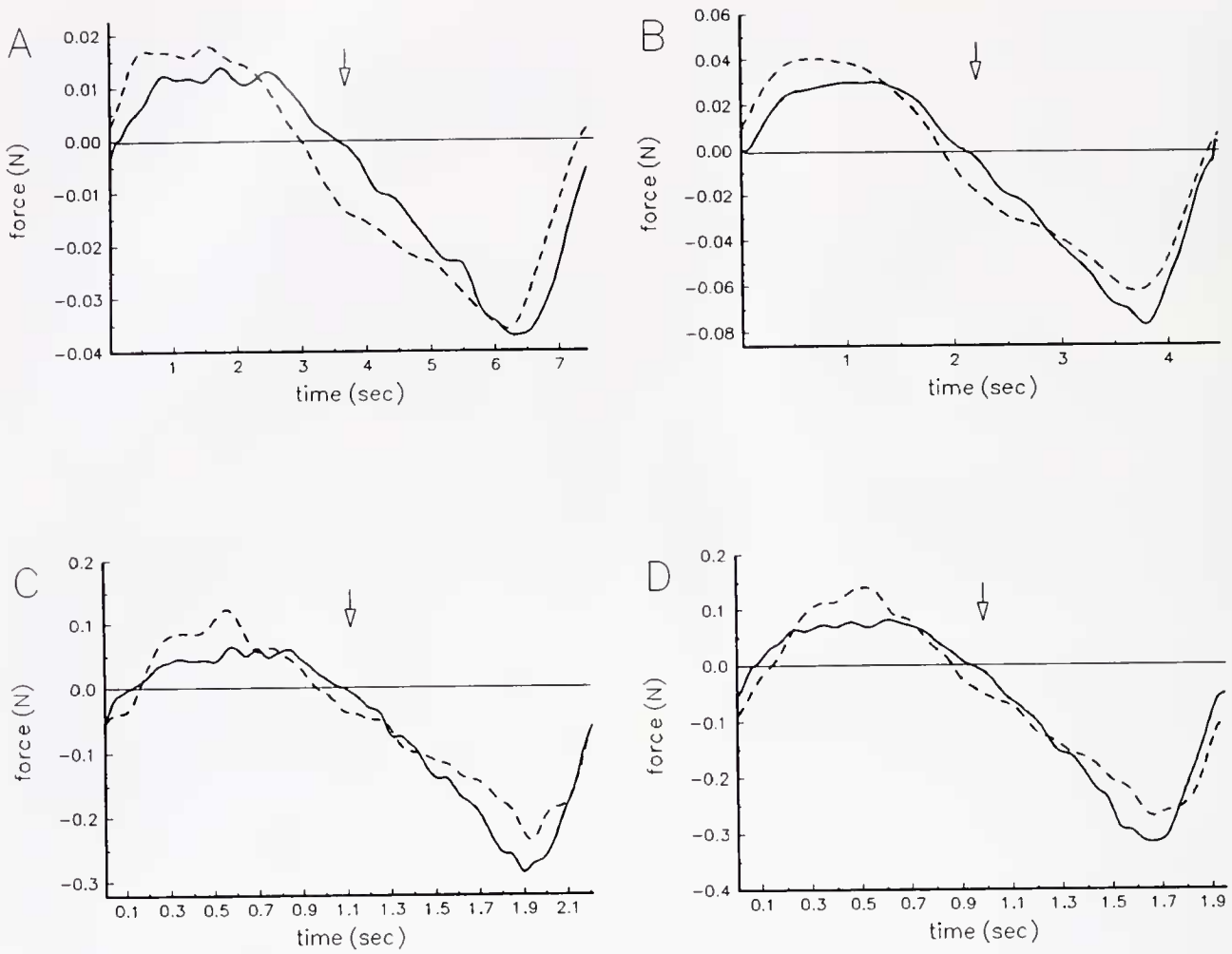

Figure 4. Comparison of thrust generated by the model (dotted lines) with thrust calculated on the basis of the same frequency and speed using eqn. 6 (solid lines). Each graph represents a single stroke of the model, although the force is averaged over all strokes during the 100 runs (and total stroke number depends on the frequency and speed). Arrows mark onset of recovery stroke. A–D correspond to the four successive larval stages the model mimics (see Table 1).

Figure 6 compares the symmetrical stroke of the model (where the fan of thin brass rods is unable to flex during the recovery stroke) with the asymmetrical stroke of the same frequency and speed (where the fan is free to flex during the recovery stroke and then opens passively during the course of the power stroke). Simulations with higher Strouhal numbers show similar patterns of thrust during the stroke. However, as the Strouhal numbers drop, the maximum thrust generated during the stroke is shifted later in the cycle, reflecting the later extension of the fan. This occurs because the model must overcome a relatively greater translational speed before it generates thrust. The result is a decrease in the relative thrust per cycle produced by the limb (as reflected by the difference between the areas under the two curves during the power stroke).

Discussion

Artemia larvae grow through a range of sizes and speeds that entail changes in the forces that determine their motions in the fluid. A physical model of the early larval propulsors, the antennae, shows that under the hydrodynamic regime experienced by the animals, these limbs generate force roughly as a cylinder at intermediate Reynolds numbers flows (eqn. 6). This empirically derived result is in agreement with a theoretical model of propulsion by copepod thoracic limbs which uses this equation to model copepod swimming by sequential movement of five pairs of appendages (Morris *et al.*, 1985).

In spite of the high frequency of the limb beat, unsteady forces are a negligible part of thrust production. Although unsteady forces are not always calculated as a source of

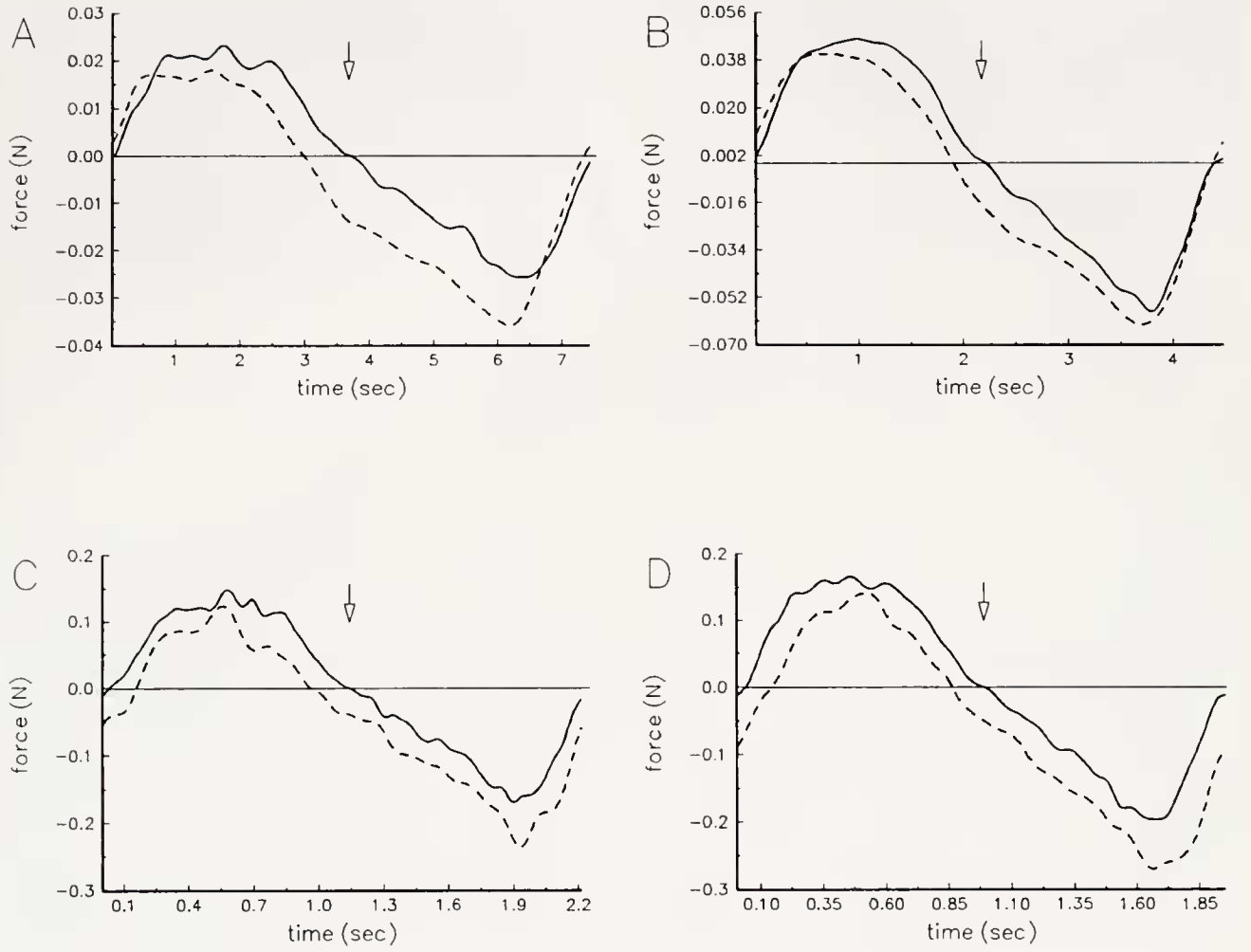

Figure 5. Comparison of thrust generated by the model (dotted lines) with thrust calculated only on the basis of the angular position of the model (solid lines). Each graph represents a single stroke of the model, although the force is averaged over all strokes during the 100 runs (and total stroke number depends on the frequency and speed). Arrows mark onset of recovery stroke. A–D correspond to the four successive larval stages the model mimics (see Table 1). In C and D there is an offset due to greater translational speeds.

thrust on oscillatory propulsors (*e.g.,* Nachtigall, 1974), Blake (1985) has shown that they may produce as much as one-third of the thrust on the limbs of water boatmen, *Cenocorixa bifida.* The Reynolds number of these animals is about two orders of magnitude higher than those experienced by *Artemia* larvae modeled here (600 *vs.* 1–9), so it is not surprising that unsteady forces are correspondingly greater.

Although the model does not capture all of the details of the animal's limb kinematics, it does provide some generalizations about oscillating propulsion. In an overview of swimming in crustaceans, Hessler (1985) hypothesizes that setal structures on diverse swimming limbs may extend passively. Such passive extension is the case for the feeding setae of a filter-feeding shrimp (Fryer, 1977). This passive behavior may be possible only in some hydrodynamic regimes. At the intermediate Reynolds numbers modeled here, comparison of the thrust generated by the model at low and high Strouhal numbers suggests that an animal could use passively extending setae only if the speed of limb oscillation is high relative to the forward speed of the body—otherwise a passively extending system provides little thrust for propulsion. However, real setae are not accurately modeled by a metal wire fan. Typically, setal diameter varies from base to tip, and setal morphology is asymmetrical in the direction of power and recovery strokes. My results suggest that the influence of both setal material and morphology on passive behavior would be worth investigating, as these could influence the time-course of thrust production in real animals.

The kinematics of the model and the kinematics of an *Artemia* antenna differ in a significant way. *Artemia* an-

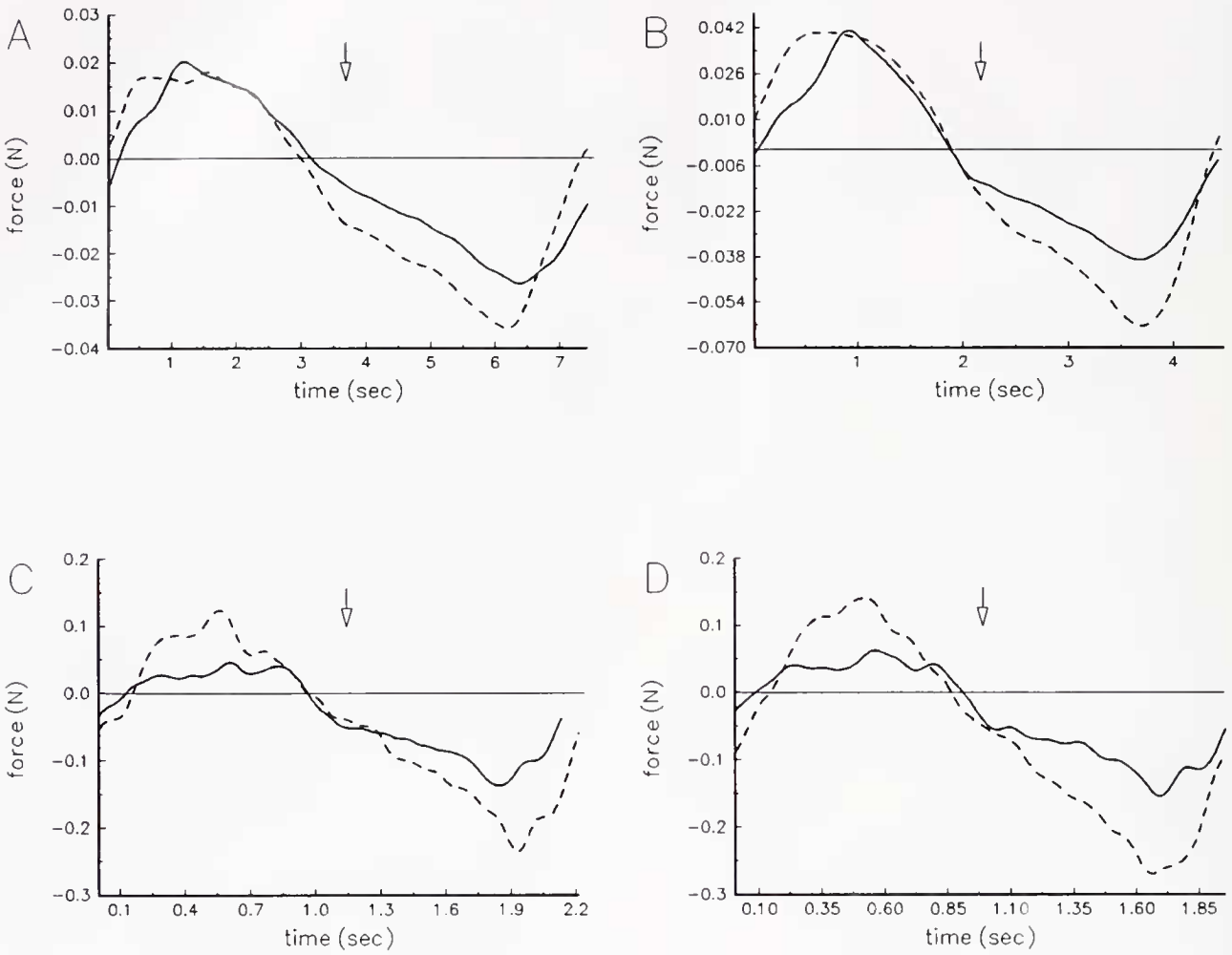

Figure 6. Thrust generated by the model when the stroke is symmetrical (dotted lines) compared with thrust generated when the stroke is asymmetrical (solid lines). Graphs represent a single stroke of the model, although the force is averaged over many strokes. Arrows mark onset of recovery stroke. A–D correspond to the four successive larval stages the model mimics (see Table I). Note that in later stages (C, D), the thrust generated during the power stroke is much smaller with an asymmetrical stroke than a symmetrical one.

tennae are linked to a freely moving body whose trajectory through the water changes as the animal develops: early stages swim in a highly pulsatile fashion; later stages do not (Williams, 1994). Therefore, unlike the model, the oscillation of the appendage is not simply coupled to a constant velocity, and the distribution of velocity along the length of the limb changes accordingly as the animal develops (Williams, 1994). Thus, the model does not provide direct information about the actual time-course of thrust production by an *Artemia* antenna during the stroke cycle. However, the force coefficient determined for the model does provide an *empirical* basis for determining drag produced by the antennal geometry moving in a fluid regime where both inertial and viscous effects determine flows. I use this empirically based force coefficient in a purely theoretical model in which I link thrust produced by a pair of appendages to resistive forces on the body and examine the mode of swimming that results (Williams, 1994).

Acknowledgments

I gratefully acknowledge grants from Sigma Xi, the Lerner-Grey fund for Marine Science, NSF grant DCB-8711654 to Tom Daniel, NSF grant BSR-8700523 to Alan Kohn. Tom Daniel, Joel Kingsolver, Alan Kohn, Garry Odell, and Dick Strathmann criticized this paper at various stages.

Literature Cited

Batchelor, G. K. 1967. *An Introduction to Fluid Mechanics.* Cambridge University Press, London. 615 pp.

Blake, R. W. 1986. Hydrodynamics of swimming in the water boatman, *Cenocorixa bifida*. *Can. J. Zool.* **64:** 1606–1613.

Daniel, T. L. 1984. Unsteady aspects of aquatic locomotion. *Am. Zool.* **24:** 121–134.

Fryer, G. 1977. Studies on the functional morphology and ecology of the aytid prawns of Dominica. *Phil. Trans R. Soc. Lond. B* **279:** 57–129.

Hessler, R. R. 1985. Swimming in Crustacea. *Trans. Roy. Soc. Edin.* **76:** 115–122.

Morris, M. J., G. Gust, and J. J. Tores. 1985. Propulsion efficiency and cost of transport for copepods: a hydromechanical model of crustacean swimming. *Mar. Biol.* **86**: 283–295.

Nachtigall, W. 1974. Locomotion, mechanics, and hydrodynamics of swimming in aquatic insects. Pp. 381–432 in *Physiology of Insecta, Vol. 3*, M. Rockstein, ed. Academic Press, New York.

Sokal, R. R., and F. J. Rohlf. 1981. *Biometry, the Principles and Practice of Statistics in Biological Research*. W. H. Freeman, San Francisco. 859 pp.

White, F. M. 1974. *Viscous Fluid Flow*. McGraw-Hill, New York. 725 pp.

Williams, T. A. 1994. A model of rowing propulsion and the ontogeny of locomotion in *Artemia* larvae. *Biol. Bull.* **187:** 164–173.